BUCKLING AND POST-BUCKLING BEHAVIOUR OF COMPOSITE CYLINDRICAL SHELLS

Chiara Bisagni
Dipartimento di Ingegneria Aerospaziale
Politecnico di Milano
Via Golgi 40, 20133 Milano, Italy
e-mail: *chiara@aero.polimi.it*

Abstract

The experimental programme presented in this paper is part of a research project aiming at improving the knowledge of the buckling behaviour of composite shell structures. In fact at present the lack of generally applicable design criteria for composite shell structures is an important factor that inhibits the efficient use of composite materials in aerospace industries, forcing the use of unduly high safety factors.
The described tests consist of axial compression and are performed on two series of nominally identical cylindrical specimens. They have two different type of lay-up orientation: cross-ply $(0°/90°)_S$ and angle-ply $(+45°/-45°)_S$, and each ply is made by kevlar cross-weaved fibres embedded into epoxy resin matrix.
An ad-hoc equipment allows to measure the geometric imperfections and the buckling pattern development on the specimens internal surfaces.
On all the surfaces measured during the tests, a two-dimensional Fourier analysis is performed, obtaining modes and amplitudes of the Fourier coefficients. They are useful to try to understand the conditions that mainly influence the buckling phenomena and to tune the numerical tools

Introduction

The insufficient availability of design criteria for composite structures has largely restricted the efficient use of composite materials in aerospace, marine and civil industry. The gap is particularly severe in buckling strength prediction of composite shell structures.

Even the buckling behaviour of isotropic shells [1] [2] [3] depends on a wide range of parameters and this is much more complicated in the case of composite shells. Many studies concerning this field of research have been presented [4] [5] [6], but they have not led to systematic and widely applicable design criteria and are therefore of limited use to practising engineers. An extensive programme, combining experimental, numerical and analytical activities can help to deeply understand the shells buckling phenomena.
Here are presented the results of axial compression tests performed on composite cylindrical shells. An ad-hoc equipment allows to measure the geometric imperfections and the buckling pattern development on the specimens internal surfaces. The possibility to test series of nominally identical specimens allows an assessment of the repeatability of the buckling tests. All the possible information regarding displacements, stresses and geometric imperfections are recorded.
They are useful to try to understand the conditions that mainly influence the buckling phenomena and to tune the numerical tools. In fact the tuning of the numerical and analytical tools using the test results will allow a wider parametric study to be performed, useful for the definition of strength design criteria.

Specimen characteristics

The available specimens (see Figure 1) have the following geometric properties:

Length (mm)	700
Radius (mm)	350
Thickness (mm)	1.04

They present two thicker reinforced ends at the top and bottom to facilitate the fixing into the loading rig. The actual length is therefore limited to the central part of the cylinder and is equal to 540 mm.

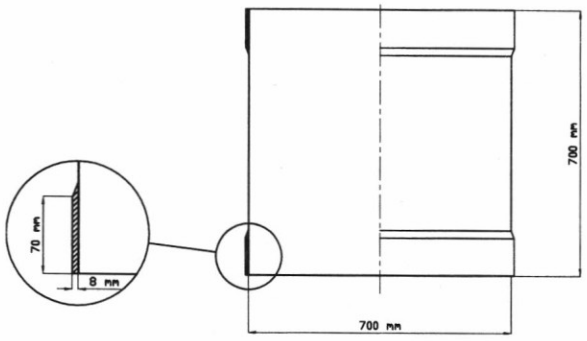

FIGURE 1 - Cylindrical specimen

Each ply of the specimens is made by kevlar cross-weaved fibres embedded into epoxy resin matrix and has the following properties, where x_1 and x_2 are the orthogonal in-plane axes:

E_{11} (N/mm^2)	23450
E_{22} (N/mm^2)	23450
G_{12} (N/mm^2)	1520
G_{13} (N/mm^2)	1520
G_{23} (N/mm^2)	1520
ν_{12}	0.2
ρ, density (kg/mm^3)	1.32×10^{-6}
t, thickness (mm)	0.26

The tested specimens present two different types of lay-up orientation: cross-ply $(0°/90°)_S$ and angle-ply $(+45°/-45°)_S$.

Loading rig

The loading rig is shown in Figure 2. The axial force is provided by an hydraulic ram, but the actual load applied to the specimen is controlled by four adjustable screw stops, acting on the four corners of the loading platform. Thus, the loading machine is displacement controlled with a good accuracy.
The compression load and the axial displacement are measured, during the test, on three equally spaced points. This gives a measure of the accuracy of the loading process, in terms of load and displacement uniformity.

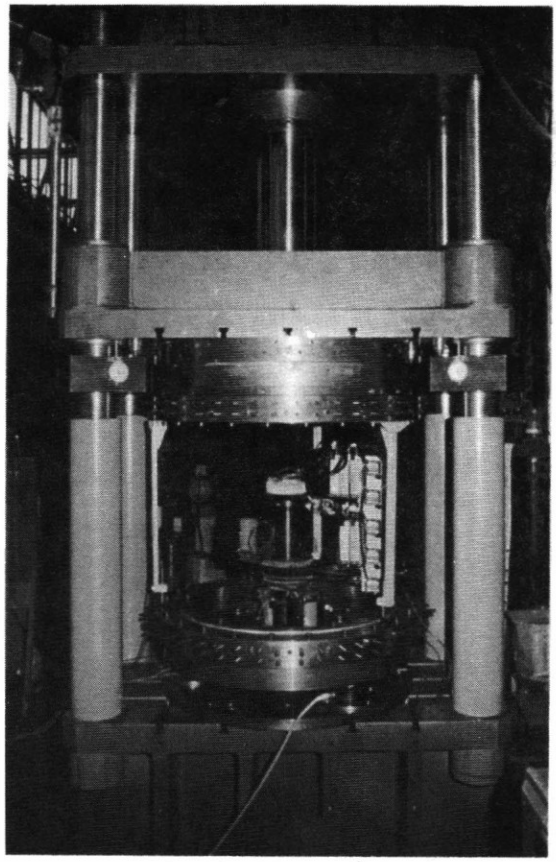

FIGURE 2 - Loading rig

The compression load is measured by three load cells, located under the lower clamp. The axial shortening is measured by three LVDT transducers. They are placed on three vertical bars, fixed on the upper clamp, and they operate on the lower clamp, allowing to measure the distance between the clamps, representing the specimen's displacement. In this way it is possible to monitor, during the test, both the load and displacement actually applied.
The clamping system of the specimens to the loading rig is very important, because it is need not to create any internal stress during the clamp. The used system is a mechanical system, where both upper and lower sides of the specimen are fixed to the loading rig, by pressing the reinforced end of the cylinder, through 24 external steel cylindrical sectors, against an internal knurled steel ring. The clamping force has an uniform distribution, because there are 4 screws for each sectors and because the sectors are tighted, in a crossed way, with 3 subsequent moment levels, controlled by a dynamometer wrench. In each sector there is also a screw for pulling back the sector and setting free the specimen.

Equipment for the buckling tests

An ad-hoc equipment [7], that allows to measure the geometric imperfections and the buckling pattern development on the specimens internal surfaces, has been designed and constructed. It is schematically represented in Figure 3.

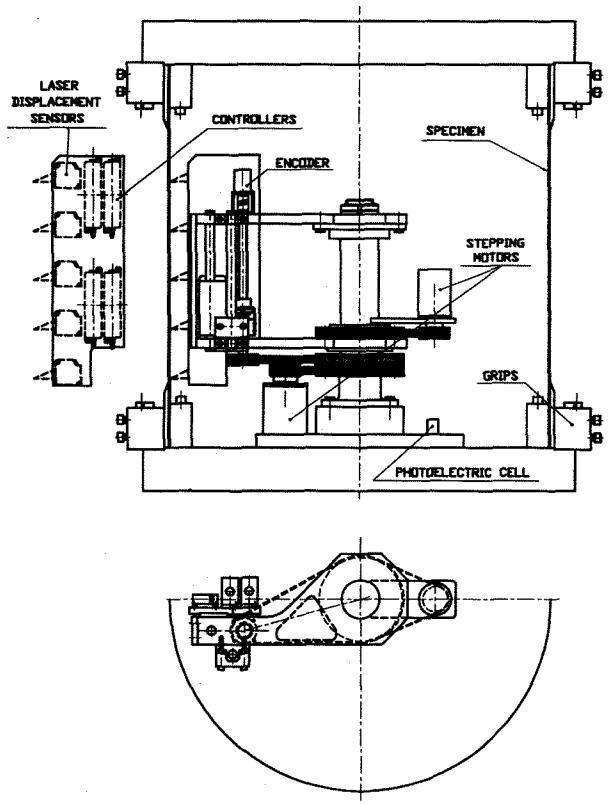

FIGURE 3 - Experimental equipment

The equipment consists of a central cylindrical body, connected with a circular plate, fixed in the middle of the specimen lower clamp. In this cylindrical body, used as a support, there are four precision bearings, free to rotate. On these bearings, two arms, with no relative movement, are binded. The arms support the slide, where five laser displacement sensors are placed.
The slide has the possibility to rotate and to vertically translate, through a worm screw. These movements are given by two stepping motors, fixed on the support. The first stepping motor is binded through a toothed belt to a pulley, connected with the two arms and it gives the rotation of the sensors round the vertical axis. The second stepping motor is connected, always through a toothed belt, to a double idle pulley on the central support. The pulley sends back the movement to a pulley fixed on the worm screw, giving the translation of the slide.

The vertical position of the slide is known by an incremental encoder, connected to the worm screw. The starting of every data acquisition is regulated by a photoelectric cell, that allows to start the data acquisition always from the same point.
The five laser displacement sensors are placed at the distance of 40 mm from the specimen internal surface. They have a measurement range of ±10 mm, with a resolution that depends on the acquisition speed (for acquisition every 2 ms the resolution is 15 μm). So they allow to record both the geometric imperfections, that are some tens of micrometers, and the buckling pattern, showing displacements of about 10-20 mm. During previous tests LVDT transducers were used, but the laser sensors present a great advantage, since avoiding any contact with the specimen surface they don't influence at all the buckling stresses.

Tests results

During the cylinder's buckling test, the compression load and the axial displacement are measured and visualised on the computer's screen. A typical diagram of the compression load versus average axial displacement for a cross-ply cylinder is reported in Figure 4.

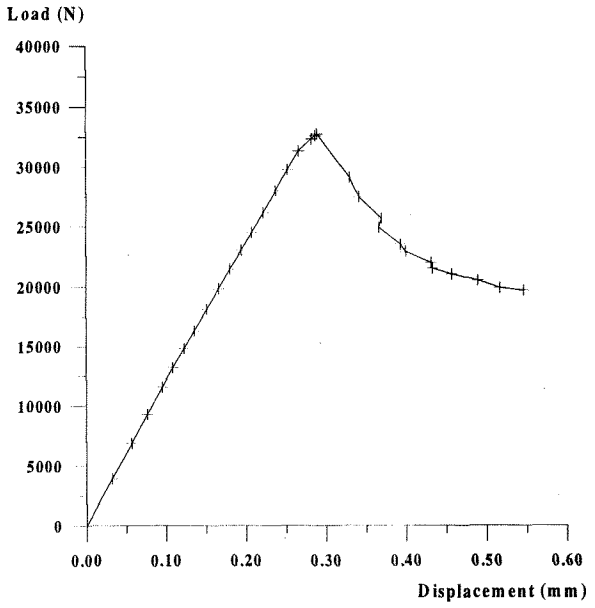

FIGURE 4 - Cross-ply cylinder: compression load versus displacement

During all the tests performed on the cross-ply cylinders, the measured buckling load was between 32000 N and 34000 N and these values are about the 85-88% of the theoretical linear

buckling loads. The buckling load is always reached without significant pre-buckling nonlinearities and the post-buckling curve approximately reaches the 50% of the limit load.

The buckling load of the angle-ply cylinders is in the same range of values, but the load-displacement diagram present bigger displacements. The Figure 5 show a typical diagram for an angle-ply cylinder, where both loading and unloading sequences are reported.

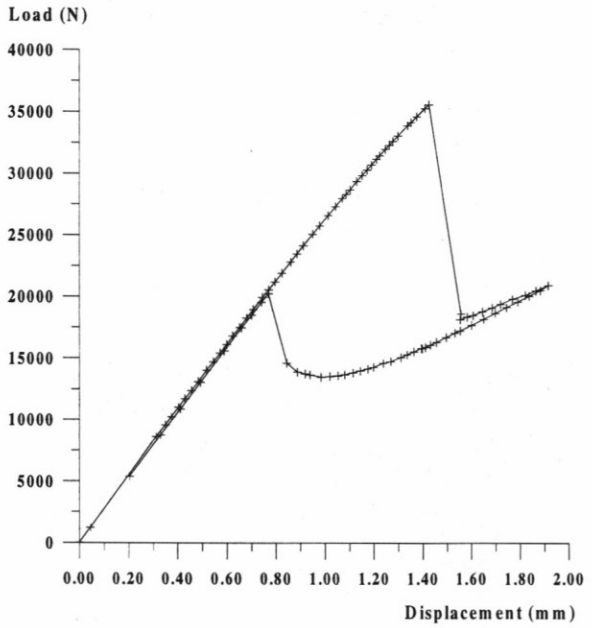

FIGURE 5 - Angle-ply cylinder: compression load versus displacement

The ad-hoc equipment allows to record the cylinder's internal surface about 15-25 times during a buckling test, by means of a dedicated software, that controls the rotatory and vertical movements of the laser sensors and their positions and starts the measures. The time required to measure a complete surface is 4 minutes.
The acquisitions are made along circumferences, shifting the laser sensors from one to another with an helicoidal movement. So the measures are taken in equally spaced points on the circumferences and placed on equally spaced circumferences and it is possible to regulate, with an extreme flexibility, the sampling pitch in both directions.
The internal surfaces measurements are recorded in a regular mesh of points 10 mm spaced both circumferentially and axially, resulting 220 measures along any circumference and 46 measures along any meridian. The measurements are limited to the central part of the cylinder surface and the covered area has a length of 450 mm, being therefore shorter than the actual meridian length of 540 mm.

Some cross-ply cylinder's internal surfaces measured during the same buckling test are reported below. The internal surface is measured before the test (see Figure 6), allowing to know the geometric imperfections.

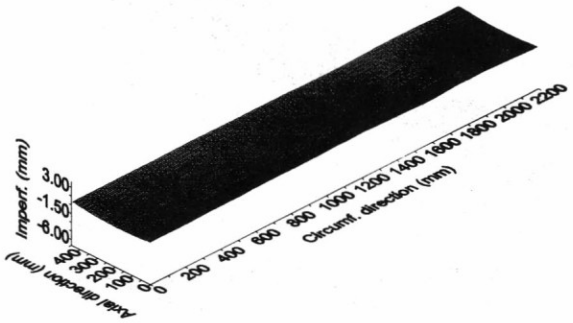

FIGURE 6 - Cross-ply internal surface before the test

During the pre-buckling, the surface is normally acquired every 5000 N and then, more frequently, approaching the critical load. No differences are noted among the surfaces measured in the pre-buckling.
At the critical load the first development of the buckling pattern is visible (see Figure 7).

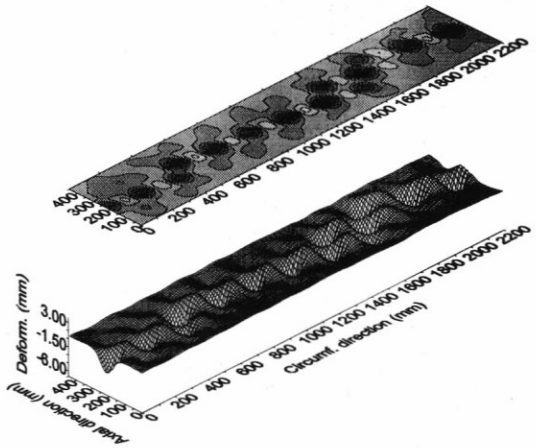

FIGURE 7 - Cross-ply internal surface at 29090 N - 0.330 mm

The buckling pattern is expanding regularly in post-buckling, until when the pattern is defined and there is only a depth's growth. At the maximum cylinder axial displacement (see Figure 8), it is possible to point out about 11 circumferential waves and 2 axial waves. The displacements

normal to the surface reach 7 mm internally and 4 mm externally.

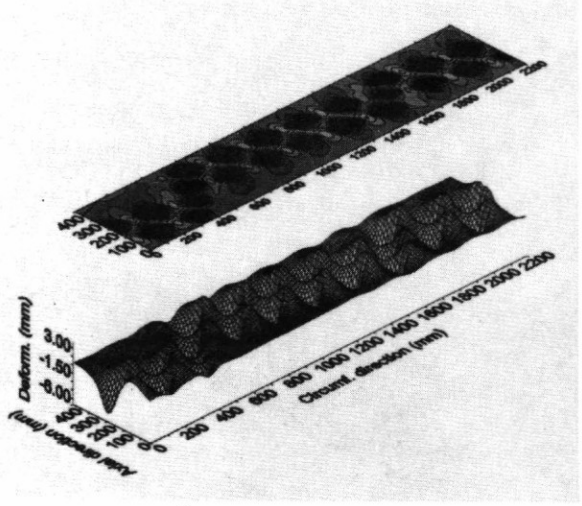

FIGURE 8 - Cross-ply internal surface at 19670 N - 0.546 mm

After the unloading, the cylinder maintains a negligible deformation (see Figure 9), that however disappears in the surface measured the day after the test. The unloading is therefore completely elastic.

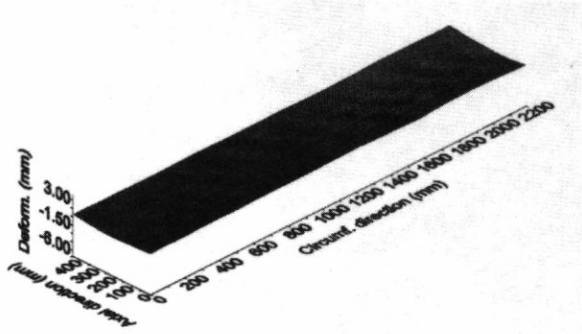

FIGURE 9 - Cross-ply internal surface after the test

Also for the angle-ply cylinders, no differences are noted among the surfaces measured in the pre-buckling. On the contrary, a well-defined pattern is developed immediately after the buckling load (see Figure 10). This pattern doesn't significantly change in the post-buckling. The waves are here 8 circumferentially and only 1 axially. The displacements normal to the surface are bigger than those of the cross-ply cylinders; they reach 11 mm internally and 5 mm externally. Also for the angle-ply cylinders, the unloading is completely elastic.

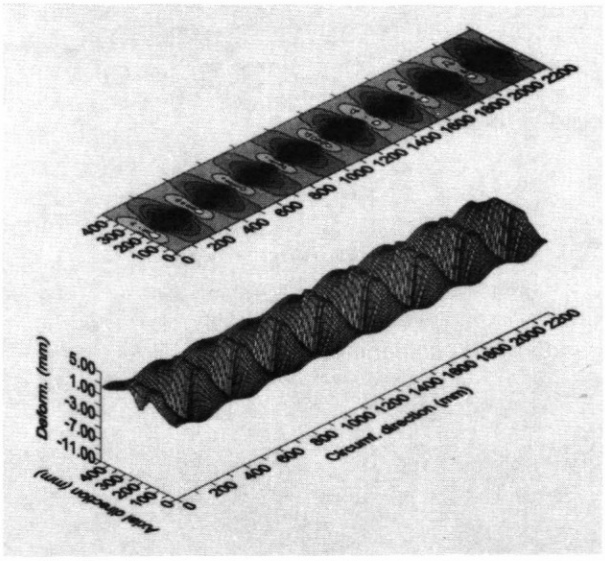

FIGURE 10 - Angle-ply internal surface at 18620 N - 1.558 mm

In Figure 11 a photograph of a typical buckling pattern for a cross-ply cylinder is reported.

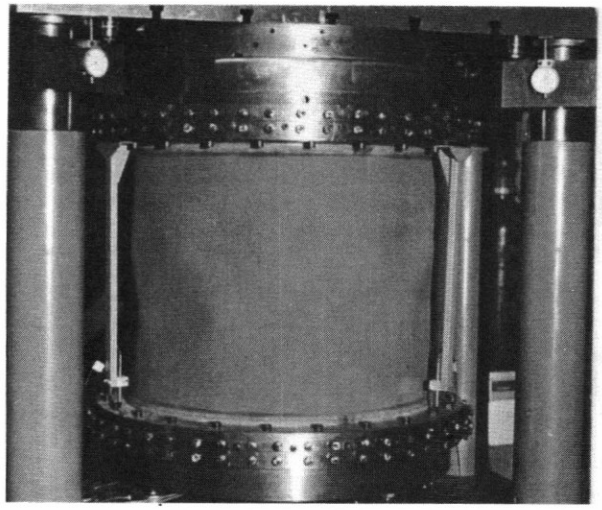

FIGURE 11 - Typical buckling pattern for a cross-ply cylinder

Two-dimensional Fourier analysis

A two-dimensional Fourier analysis [8] [9] [10] has been performed on each internal surface measured during a buckling test, obtaining modes and amplitudes of the Fourier coefficients.
In Figure 12 the Fourier decompositions of some surfaces of the same buckling test on a cross-ply cylinder are reported. Initially only the geometric imperfections modes are present and then the buckling pattern modes become significant.
The same analysis for an angle-ply cylinder is reported in Figure 13.

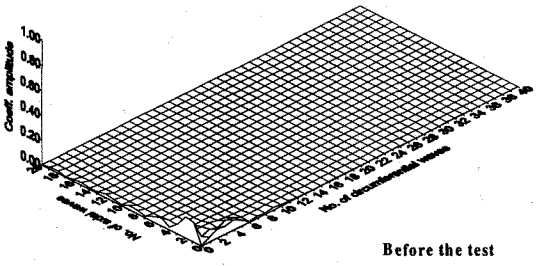

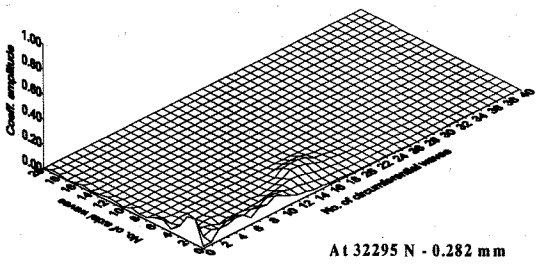

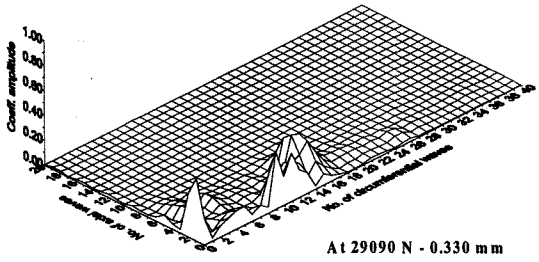

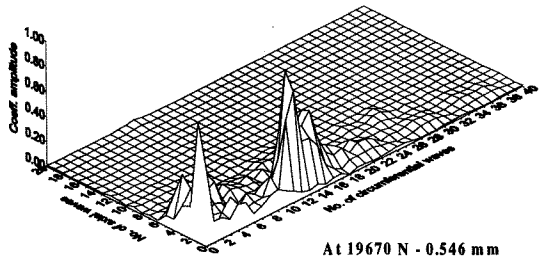

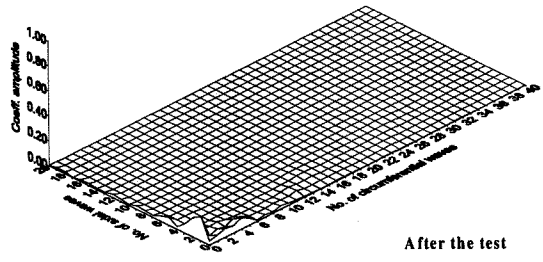

FIGURE 12 - Fourier decomposition of some surfaces measured during the same buckling test (cross-ply cylinder)

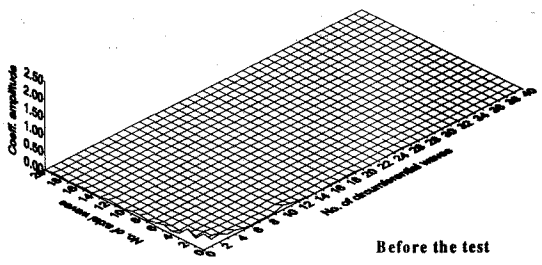

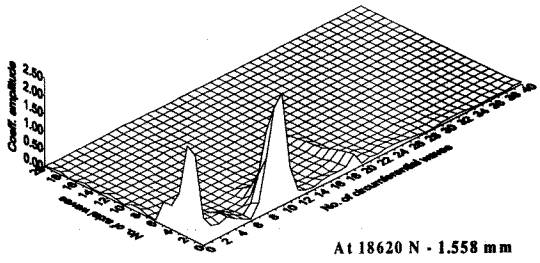

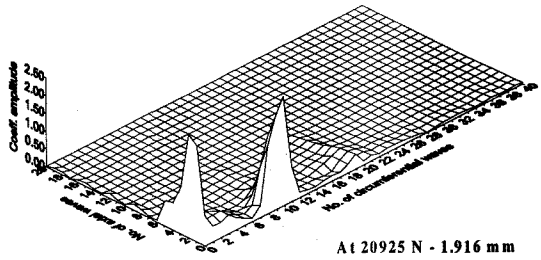

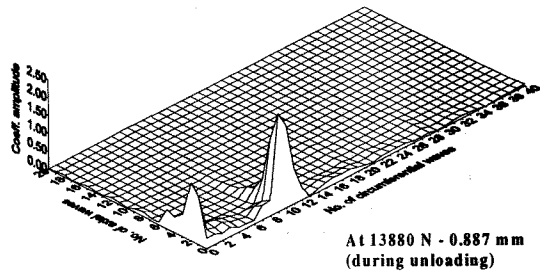

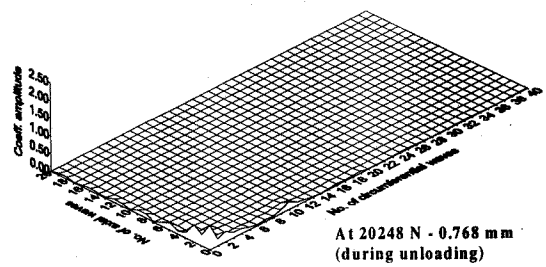

FIGURE 13 - Fourier decomposition of some surfaces measured during the same buckling test (angle-ply cylinder)

In Figure 14 the modal amplitude versus the cross-ply cylinder's axial displacement, for some given axial and circumferential wave numbers, are reported.

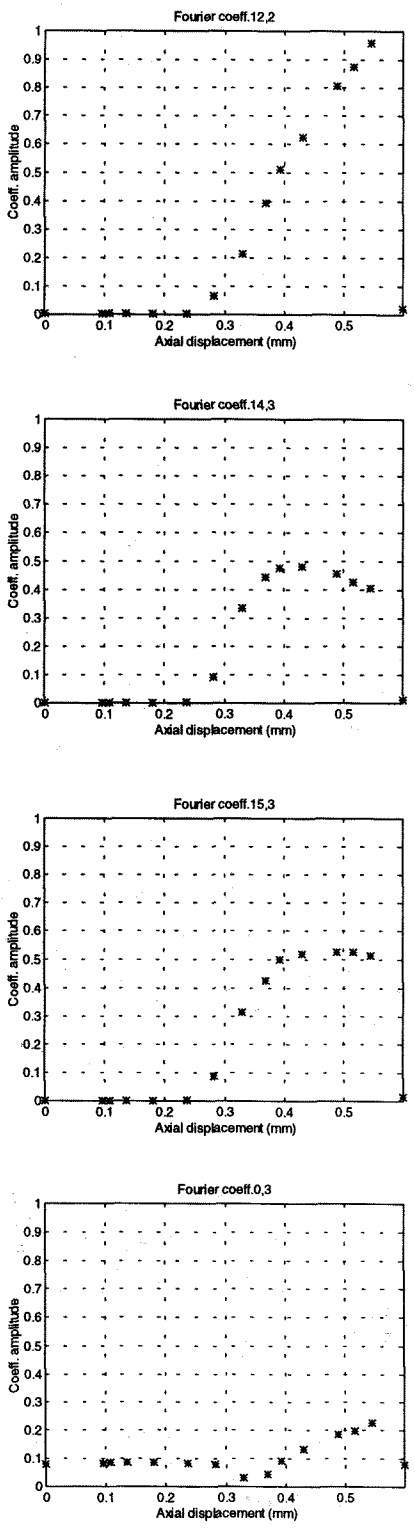

FIGURE 14 - Some Fourier coefficient (cross-ply cylinder)

The surfaces here analysed are the surfaces measured during the loading and one measured after the test, when the cylinder is completely unloaded.

For the cross-ply cylinders, some modes, for example the mode (12,2), develop during the buckling and increase with a parabolic trend. They are present with a small amplitude after the test. Other modes, for example the modes (14,3) and (15,3), develop at the beginning of the buckling, but they initially grow and then decrease.

The geometric imperfection modes, for example the mode (0,3), grow during the buckling, but not in a regular way.

In Figure 15 the modal amplitude versus the angle-ply cylinder's axial displacement for some given axial and circumferential wave numbers are reported. In this case only the surfaces measured during the loading are analysed.

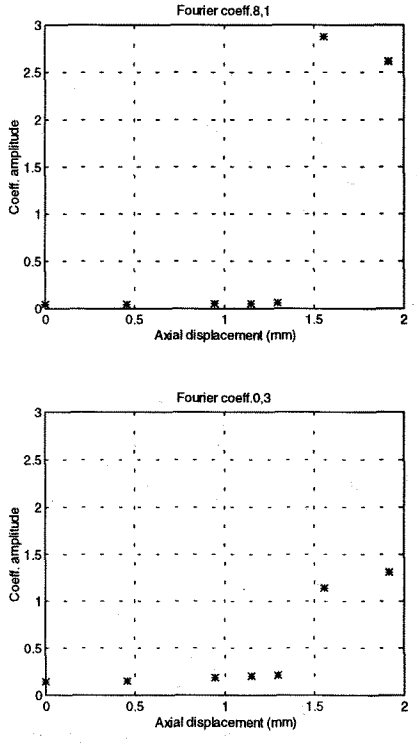

FIGURE 15 - Some Fourier coefficient (angle-ply cylinder)

For the angle-ply cylinder the modes are better defined then for the cross-ply cylinders. Here the mode (8,1) is pointed out. Also the geometric imperfection modes, for example the mode (0,3), grow during the buckling in a regular way.

Conclusions

An extensive experimental project of buckling tests on two series of nominally identical composite cylindrical shells under axial compression has been here presented. An ad-hoc equipment has allowed to measure the geometric imperfections and to follow the buckling pattern development on the specimens internal surfaces.
A two-dimensional Fourier analysis has been performed on the surfaces recorded during the tests. This analysis, based on all the recorded information, will help in the tuning of the numerical and analytical tools, allowing a wider parametric study to be performed useful for the definition of strength design criteria.
The experimental programme will be extended also to torsion and combinations of axial compression and torsion and will cover cylindrical shells with other lay-up configurations and made by other types of composite materials.

Bibliography

1. Kollar L., Dulacska E., *"Buckling of shells for engineers"*, John Wiley & Sons, 1984
2. Brush D.O., Almroth A., *"Buckling of bars, plates and shells"*, Mc. Graw Hill, New York, 1975
3. Koiter W.T., A translation of *"The stability of elastic equilibrium"*, Technical Report AFFDL-TR-70 25, 1970
4. Jullien J.F., *"Buckling of shell structures on land, in the sea and in the air"*, Lyon Symposium, Elsevier Applied Science, 1991
5. Jun S.M., Hond C.S., *"Buckling behaviour of laminated composite cylindrical panels under axial compression"*, Computers and Structures, 1988
6. Giavotto V., Poggi C., Chryssanthopoulos M., *"Buckling of imperfect composite shells under compression and torsion"*, Proc. of Int. Meeting on Rotorcraft Basic Research, Atlanta, 1991
7. Bisagni C., *"Instabilità di gusci cilindrici in materiale composito"*, Proc. of AIDAA - XIII National Congress, Roma, 1995
8. Brigham E. O., *"Fast Fourier Transform"*, Prentice Hall
9. Nachtigal C. L., Martin M. D., *"Instrumentation and control: foundamentals and applications"*, New York, Wiley & Sons, 1990
10. Bendat J. S., Piersol A.G., *"Engineering applications of correlation and spectral analysis"*, New York, Wiley & Sons, 1993